

# Effect of spectral modification of $\rho$ on shear viscosity of a pion gas

Sukanya Mitra, Sabyasachi Ghosh, and Sourav Sarkar

*Theoretical Physics Division, Variable Energy Cyclotron Centre,*

*1/AF Bidhannagar Kolkata - 700064, India*

## Abstract

We evaluate the shear viscosity of a pion gas in the relativistic kinetic theory approach. The in-medium propagator of the  $\rho$  meson at finite temperature is used to evaluate the  $\pi - \pi$  scattering amplitude in the medium. The real and imaginary parts of the self-energy calculated from one-loop diagrams are seen to have noticeable effects on the scattering cross-section. The consequences on temperature dependence of the shear viscosity evaluated in the Chapman-Enskog and relaxation time approximations are studied.

## I. INTRODUCTION

One of the most exciting revelations that has emerged from experiments at the Relativistic Heavy Ion Collider (RHIC) is the strongly interacting nature [1] of the produced matter. It has properties of an almost perfect fluid characterized by a rather small value of the shear viscosity over entropy density ratio  $\eta/s$ , close to the quantum or KSS bound [2]. This interpretation based on the measured elliptic flow  $v_2$  of hadrons in terms of viscous hydrodynamics however depends sensitively on the value of  $\eta/s$ . A lot of interest has been generated leading to quite a few estimates of the transport coefficients of both partonic [3, 4] as well as hadronic [5–11] constituents of strongly interacting matter. In general, the shear viscosity coefficient is inversely proportional to the cross-section leading to strongly interacting systems being less viscous than non-interacting ones, the larger values of the viscous coefficients resulting from the possibility of momentum transport over larger distances in the latter case. The interaction cross-section thus plays the pivotal role in the relaxation of systems towards equilibrium.

Pions form the most important component in a hadronic system. There have been quite a few estimates of the viscosity of a pion gas. Almost all these calculations have been performed in the relativistic kinetic theory approach in which a crucial input is the  $\pi\pi$  differential cross-section. In [6, 9], the scattering amplitude was estimated from the lowest order Lagrangian of chiral perturbation theory [12, 13] and in [7] a unitarized amplitude was employed for a meson gas. Phenomenological amplitudes obtained from fits to phase shift data have been employed in [10] in view of the fact that the  $\pi\pi$  cross-section estimated from lowest order chiral perturbation theory is known to deviate from the experimental data beyond centre of mass energy of 500 MeV primarily due to the  $\rho$  pole which dominates the cross-section in the energy region between 500-1000 MeV.

The spectral modification of the  $\rho$  in hot and dense matter is known to play the most important role in explaining the invariant mass spectra of lepton pairs from relativistic heavy ion collisions in the region below the nominal  $\rho$  mass [14–16]. The lepton pair production in this region is related by vector meson dominance to two-pion annihilation proceeding through  $\rho$ -exchange. Moreover, medium modification of the  $\rho$  spectral function incorporated in the evaluation of elliptic flow of lepton pairs of low invariant mass have been recently shown [17] to result in values close to those of hadrons of similar mass, ascertaining the role of  $v_2$  of

hadrons in describing the early stages of heavy ion collisions. It is natural to extend this scenario to the evaluation of the transport coefficients, the temperature dependence of which is particularly relevant for the electromagnetic probes which are emitted at all stages of the collision spanning a range temperatures. Investigations with temperature dependent  $\pi\pi$  cross-section involving  $\sigma$  exchange have recently been addressed in [18]. Our intention in this work is to observe the effect of the in-medium spectral function of the  $\rho$  on the shear viscosity of a pion gas.

The first task is to obtain the energy dependent  $\pi\pi$  cross-section using a phenomenological approach which is close to the experimental value and at the same time is theoretically amenable to the incorporation of medium effects. To this end we consider the scattering to proceed via  $\rho$  exchange for which the invariant amplitude is evaluated using effective interactions. Medium effects on  $\rho$  propagation are introduced through one-loop self-energies to obtain the modified cross-section at finite temperature. These are discussed in section II. The corresponding effect on the shear viscosity of a pion gas is the subject of section III where it is evaluated using the non-relativistic, Chapman-Enskog and relaxation time approximations. We end with a summary in section IV. Details of the calculation of the  $\rho$  self-energy in the medium has been summarized in the Appendix.

## II. THE $\pi\pi$ CROSS-SECTION WITH MEDIUM EFFECTS

We evaluate the invariant amplitude for  $\pi\pi$  scattering using an effective Lagrangian in which the coupling of the  $\rho$  meson to the pions is introduced through the gauge covariant derivative of the pion field operator to obtain [19]

$$\mathcal{L}_{\rho\pi\pi} = \frac{ig_\rho}{4} Tr[V^\mu, [\partial_\mu\Phi, \Phi]] \quad (1)$$

where  $Tr$  indicates trace in  $SU(2)$  space. The matrix  $\Phi$  collects the pion fields in the form  $\begin{pmatrix} \pi^0 & \sqrt{2}\pi^+ \\ \sqrt{2}\pi^- & -\pi^0 \end{pmatrix}$  and  $V^\mu$  collects the  $\rho$  meson fields analogously. The coupling constant  $g_\rho=6.05$  is fixed from the  $\rho \rightarrow \pi\pi$  decay width. This interaction leads to  $\pi\pi$  scattering diagrams with  $\rho$  exchange in the  $s$ ,  $t$  and  $u$  channels. In these calculations we modify the  $\rho$  propagator  $D_{\mu\nu}^{(0)} = (-g_{\mu\nu} + q_\mu q_\nu / m_\rho^2) / (q^2 - m_\rho^2 + i\epsilon)$  replacing  $i\epsilon$  with  $im_\rho\Gamma_\rho(s)$  where the two-pion decay width is  $\Gamma_\rho(s) = \frac{g_\rho^2}{48\pi s}(s - 4m_\pi^2)^{3/2}$ . This is done only for  $s$ -channel  $\rho$ -exchange diagrams which contribute only in the case of total isospin  $I = 1$ .

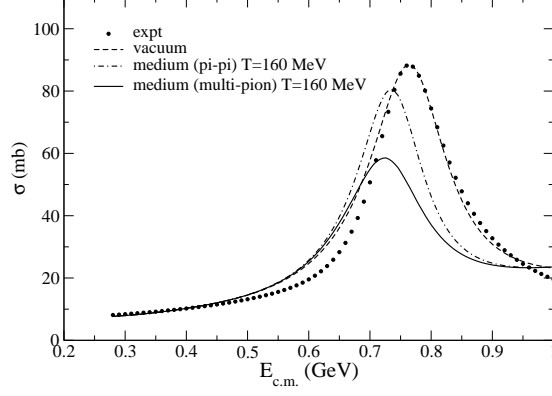


FIG. 1: The  $\pi\pi$  cross-section as a function of centre of mass energy. The dashed line indicates the cross-section obtained using eq. 2 which agrees well with the experimental values shown by filled circles. The dash-dotted and solid lines depict the in-medium cross-section for  $\pi\pi$  and multi-pion loops respectively in the  $\rho$  self-energy evaluated at  $T=160$  MeV.

In order to describe  $\pi\pi$  scattering at low energies it is essential to also include  $\sigma$ -exchange diagrams. We use the interaction  $\mathcal{L}_{\sigma\pi\pi} = \frac{1}{2}g_\sigma m_\sigma \vec{\pi} \cdot \vec{\pi} \sigma$  with  $g_\sigma = 2.5$  to calculate the scattering amplitudes where as before we have introduced the  $\sigma$  width in the  $s$ -channel diagram which now appear only for  $I = 0$ . The values  $m_\sigma = 450$  MeV and  $\Gamma_\sigma = 550$  MeV that we use are in conformity with estimates in [20]. Going over from the charge to the isospin basis it is easy to write down the matrix elements for all the possible values of the total isospin of the two pions. They are,

$$\begin{aligned}
\mathcal{M}_{I=0} &= 2g_\rho^2 \left[ \frac{s-u}{t-m_\rho^2} + \frac{s-t}{u-m_\rho^2} \right] + g_\sigma^2 m_\sigma^2 \left[ \frac{3}{s-m_\sigma^2 + im_\sigma \Gamma_\sigma} + \frac{1}{t-m_\sigma^2} + \frac{1}{u-m_\sigma^2} \right] \\
\mathcal{M}_{I=1} &= g_\rho^2 \left[ \frac{2(t-u)}{s-m_\rho^2 + im_\rho \Gamma_\rho(s)} + \frac{t-s}{u-m_\rho^2} - \frac{u-s}{t-m_\rho^2} \right] + g_\sigma^2 m_\sigma^2 \left[ \frac{1}{t-m_\sigma^2} - \frac{1}{u-m_\sigma^2} \right] \\
\mathcal{M}_{I=2} &= g_\rho^2 \left[ \frac{u-s}{t-m_\rho^2} + \frac{t-s}{u-m_\rho^2} \right] + g_\sigma^2 m_\sigma^2 \left[ \frac{1}{t-m_\sigma^2} + \frac{1}{u-m_\sigma^2} \right]. \quad (2)
\end{aligned}$$

The differential cross-section is then obtained from  $\frac{d\sigma}{d\Omega} = |\overline{\mathcal{M}}|^2 / 64\pi^2 s$  where the isospin averaged amplitude is given by  $|\overline{\mathcal{M}}|^2 = \frac{1}{9} \sum (2I+1) |\overline{\mathcal{M}}_I|^2$ . Ignoring the  $I = 2$  contribution, the integrated cross-section (with an additional factor of 1/2 for identical particles) plotted as a function of the centre of mass energy in Fig. 1 (dashed line) is seen to agree reasonably well with the one taken from Ref. [21] (shown by filled circles) which corresponds to a resonance saturation parametrization of isoscalar and isovector phase shifts obtained from various empirical data involving the  $\pi\pi$  system. We will use this theoretical estimate as a

benchmark to study medium effects.

The effect of the medium on  $\rho$  propagation is quantified through its self-energy. The standard procedure is to evaluate this quantity by perturbative methods using effective interactions and then obtain the exact propagator using the Dyson equation, depicted pictorially in Fig. 2. We now recollect the main steps in this scheme omitting details which have been explicitly given in [22, 23]. In the real time formulation of thermal field theory, all two-point functions assume a  $2 \times 2$  matrix form [24] which can be diagonalized. The diagonal components also obey the Dyson equation [25] by means of which the full propagator  $D_{\mu\nu}$  is obtained as

$$D_{\mu\nu} = D_{\mu\nu}^{(0)} + D_{\mu\sigma}^{(0)} \Pi^{\sigma\lambda} D_{\lambda\nu} \quad (3)$$

where  $D_{\mu\nu}^{(0)}$  is the vacuum propagator for the  $\rho$  meson and  $\Pi^{\sigma\lambda}$  is the self energy function obtained from one-loop diagrams shown in Fig. 2. Following [22, 24] we write the in-medium self-energy in terms of longitudinal and transverse parts

$$\Pi_{\mu\nu} = P_{\mu\nu} \Pi^T + Q_{\mu\nu} \Pi^L \quad (4)$$

where  $P_{\mu\nu}$  and  $Q_{\mu\nu}$  are the transverse and longitudinal projection tensors respectively. These are defined as [22]

$$P_{\mu\nu} = -g_{\mu\nu} + \frac{q_\mu q_\nu}{q^2} - \frac{q^2}{\bar{q}^2} \tilde{u}_\mu \tilde{u}_\nu, \quad \tilde{u}_\mu = u_\mu - (u \cdot q) q_\mu / q^2 \quad (5)$$

and

$$Q_{\mu\nu} = \frac{(q^2)^2}{\bar{q}^2} \tilde{u}_\mu \tilde{u}_\nu, \quad \bar{q}^2 = (u \cdot q)^2 - q^2. \quad (6)$$

where  $u_\mu$  is four velocity of the thermal bath. It is easy to see that

$$P_{\mu\nu} + Q_{\mu\nu}/q^2 = -g_{\mu\nu} + q_\mu q_\nu / q^2. \quad (7)$$

Note that while  $P$  and  $Q$  are four-dimensionally transverse,  $P$  is also three-dimensionally transverse while  $Q$  is longitudinal. Solving (3), the exact  $\rho$  propagator is obtained as

$$D_{\mu\nu}(q_0, \vec{q}) = -\frac{P_{\mu\nu}}{q^2 - m_\rho^2 - \Pi^T} - \frac{Q_{\mu\nu}/q^2}{q^2 - m_\rho^2 - q^2 \Pi^L} + \frac{q_\mu q_\nu}{m_\rho^2 q^2} \quad (8)$$

where  $\Pi^T$  and  $\Pi^L$  can be obtained from the relations

$$\Pi^T = -\frac{1}{2}(\Pi_\mu^\mu + \frac{q^2}{\bar{q}^2} \Pi_{00}), \quad \Pi^L = \frac{1}{\bar{q}^2} \Pi_{00}, \quad \Pi_{00} \equiv u^\mu u^\nu \Pi_{\mu\nu}. \quad (9)$$

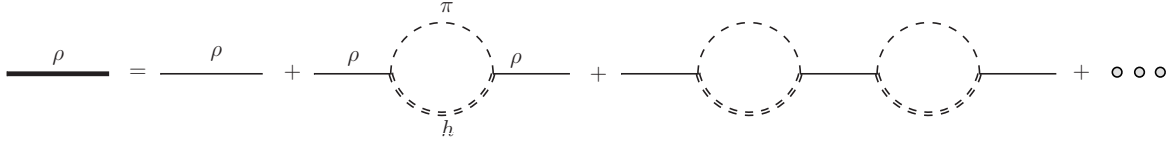


FIG. 2: The exact  $\rho$  propagator with  $\pi - h$  loop diagrams for  $h = \pi, \omega, h_1, a_1$  mesons.

As shown in [22], the three-momentum dependence of the  $\rho$  self-energy is not substantial for the present case and we can replace  $\Pi^T$  and  $q^2\Pi^L$  in the above expression by a self-energy function which is averaged over polarization. Defining this as

$$\Pi = \frac{1}{3}(2\Pi^T + q^2\Pi^L) \quad (10)$$

and neglecting the non-pole piece in (8), the in-medium propagator can be written as

$$D_{\mu\nu}(q_0, \vec{q}) = \frac{-g_{\mu\nu} + q_\mu q_\nu / q^2}{q^2 - m_\rho^2 - \text{Re}\Pi(q_0, \vec{q}) + i\text{Im}\Pi(q_0, \vec{q})} . \quad (11)$$

The real part of the self-energy modifies the pole position and the imaginary part embodies the effect of collisions and decay processes by means of which the  $\rho$  is lost or gained in the medium. Using interactions from chiral perturbation theory, the one-loop self energy was recently calculated [22]. Some details of the calculation are provided in the Appendix. The imaginary parts for  $\pi\pi$ ,  $\pi\omega$ ,  $\pi h_1$  and  $\pi a_1$  loops were obtained from the discontinuities of the self-energy in the complex energy plane. While for the  $\pi\pi$  loop, the contribution at the nominal  $\rho$  pole comes from the unitary cut, the Landau type discontinuity is responsible for contributions from loops with heavier particles. The mesons  $\omega$ ,  $h_1$  and  $a_1$  all have negative G-parity and have substantial  $3\pi$  and  $\rho\pi$  decay widths [26]. The self-energies containing these unstable particles in the loop graphs have thus been folded with their spectral functions as shown in [23]. The contributions from the loops with heavy mesons may then be considered as a multi-pion contribution to the  $\rho$  self-energy. The cross-section obtained by using the in-medium  $\rho$ -propagator (11) in place of the vacuum propagator  $D_{\mu\nu}^{(0)}$  in the evaluation of the amplitudes is shown in Fig. 1. We observe a small suppression of the peak for the  $\pi\pi$  loop and a larger effect when all the loops (indicated by multi-pion) are considered accompanied by a small shift in its position. This is due to the temperature dependence of the real and imaginary parts of the self-energy and is manifested as the modified spectral function of the  $\rho$  meson. Extension to the case of finite baryon density can be made using the results

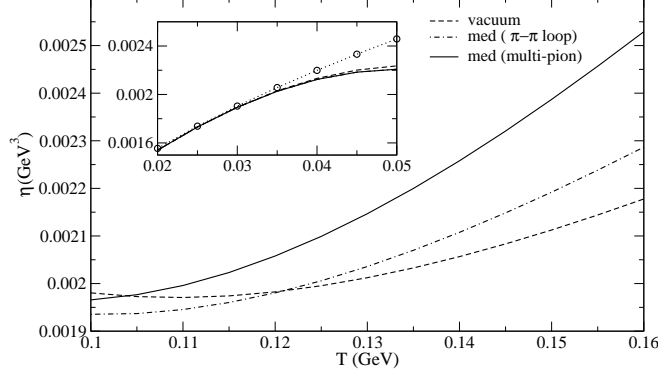


FIG. 3: The classical estimate of the shear viscosity of a pion gas as a function of temperature. The inset shows the behaviour at low temperature. The dashed line with circles depicts the  $\sqrt{T}$  behaviour at low  $T$ . The other curves in the inset are the continuations of those shown in the main figure to lower temperatures.

in [23]. Similar reduction of the  $\pi\pi$  cross-section for a hot and dense system were also obtained earlier in [27].

### III. THE SHEAR VISCOSITY OF A PION GAS

A first insight into the medium effects on the shear viscosity may be obtained by employing the classical estimate of the latter for a dilute gas of pions in terms of the mean free path  $\lambda = 1/n\bar{\sigma}$  and is given by

$$\eta \simeq \frac{1}{3} n \bar{p}(T) \lambda = \frac{\bar{p}(T)}{3\bar{\sigma}} \quad (12)$$

where the thermally averaged pion momentum and cross-section for the process  $\pi(p) + \pi(k) \rightarrow \pi(p') + \pi(k')$  are given respectively by

$$\begin{aligned} \bar{p}(T) &= \frac{\int d^3p |\vec{p}| f(E_p)}{\int d^3p f(E_p)} \\ \bar{\sigma} &= \frac{\int d^3p d^3k f(E_p) f(E_k) \sigma(s) (1 + f(E_{p'})) (1 + f(E_{k'}))}{\int d^3p d^3k f(E_p) f(E_k) (1 + f(E_{p'})) (1 + f(E_{k'}))} \end{aligned} \quad (13)$$

where  $f(E)$  denotes the Bose-Einstein distribution and  $E_p = \sqrt{\vec{p}^2 + m_\pi^2}$  and  $E_k = \sqrt{\vec{k}^2 + m_\pi^2}$ . Manipulation of the exit channel in the c.m. frame leads to  $E_{p'} = E_{k'} = E_{c.m.}/2 = \sqrt{s}/2$ . We plot the shear viscosity as a function of temperature for a range of values relevant for the hadronic phase of heavy ion collisions in Fig. 3. The behaviour of

$\eta$  in this picture is determined by the interplay of the temperature dependence of  $\bar{p}$  (which essentially behaves as  $\sqrt{T}$  since  $\bar{p}^2/2m \sim kT$ ) and that of  $\bar{\sigma}$ . A substantial effect of the reduced in-medium cross-section can be seen in this approximate estimate of  $\eta$ . In spite of possible differences in the averaging procedure, the values of  $\eta$  for the vacuum case lie within similar range with those in [10]. The behaviour at low temperatures is shown separately in the inset of Fig. 3. Since the energy of scattering decreases with  $T$  as shown in [10], the cross-section tends to a constant as the temperature is lowered (Fig. 1). The shear viscosity is then proportional to  $\sqrt{T}$ , a situation depicted by the dashed line with circles (for arbitrary proportionality constant). This  $\sqrt{T}$  behaviour of the shear viscosity at low energies has been shown analytically using a hard sphere  $\pi\pi$  cross-section in [6]. We also note in the inset that all the curves actually converge as the temperature is lowered showing that medium effects reduce with pion density.

In quantum field theory, the shear viscosity is defined using linear response in terms of the correlation function of the (spatial component) of the energy-momentum tensor which can be obtained from the Lagrangian density of the system [28, 29]. But as argued in [30, 31] a perturbative (diagrammatic) evaluation involves a sum over an infinite set of complicated diagrams in order to obtain the leading behaviour even in weakly coupled systems. A more efficient approach is to obtain these by solving the linearized transport equation.

The relativistic transport equation for the phase space distribution  $f(x, p)$  of a pion gas is written as [32]

$$p^\mu \partial_\mu f(x, p) = C[f] \quad (14)$$

where  $C[f]$  is known as the collision term. For binary elastic collisions  $p + k \rightarrow p' + k'$  the Uehling-Uhlenbeck collision term is given by

$$\begin{aligned} C[f] = & \int d\Gamma_k d\Gamma_{p'} d\Gamma_{k'} [f(x, p')f(x, k')\{1 + f(x, p)\}\{1 + f(x, k)\} \\ & - f(x, p)f(x, k)\{1 + f(x, p')\}\{1 + f(x, k')\}] W \end{aligned} \quad (15)$$

where  $d\Gamma_q = \frac{d^3q}{(2\pi)^3 q_0}$  and the collision rate  $W$  is defined as

$$W = \frac{s}{2} \frac{d\sigma}{d\Omega} (2\pi)^6 \delta^4(p + k - p' - k')$$

which includes an explicit factor of 1/2 for indistinguishable particles.

A system in local equilibrium is described by ideal fluid dynamics and departures from this state can be dealt with using dissipative dynamics. The correspondence between non-



equilibrium kinetic theory and viscous hydrodynamics can be studied by considering small departures from equilibrium. Following [33], in the first Chapman-Enskog approximation one takes the non-equilibrium distribution as

$$f(x, p) = f^{(0)}(x, p) + f^{(0)}(x, p)[1 + f^{(0)}(x, p)]\phi(x, p) \quad (16)$$

where  $f^{(0)}(x, p)$  is the local equilibrium (Bose) distribution with space-time dependent parameters and  $\phi(x, p)$  is the deviation therefrom. Putting in (14) the function  $\phi(x, p)$  is seen to satisfy the linearized transport equation

$$p^\mu \partial_\mu f^{(0)}(x, p) = -\mathcal{L}[\phi] \quad (17)$$

where

$$\begin{aligned} \mathcal{L}[\phi] = & f^{(0)} \int d\Gamma_k d\Gamma_{p'} d\Gamma_{k'} f^{(0)}(x, k) \{1 + f^{(0)}(x, p')\} \{1 + f^{(0)}(x, k')\} \\ & [\phi(x, p) + \phi(x, k) - \phi(x, p') - \phi(x, k')] W . \end{aligned} \quad (18)$$

From general considerations it can be shown that in order to be a solution of this equation, the function  $\phi$  has to be of the form  $\phi = A\partial_\mu u^\mu + C_{\mu\nu}\langle\partial^\mu u^\nu\rangle$  neglecting terms related to thermal conduction. The symbol  $\langle\cdots\rangle$  indicates a space-like symmetrized and traceless combination.

To make a connection with the coefficient of viscosity one makes use of the energy-momentum tensor given by

$$T^{\mu\nu} = \int d\Gamma_p p^\mu p^\nu f(p) . \quad (19)$$

Putting in the non-equilibrium distribution function (16) into this equation,  $T^{\mu\nu}$  separates into ideal and dissipative parts. The latter is then compared with the most general form [34, 35] for this quantity to arrive at the expression

$$\eta = -\frac{1}{10} \int d\Gamma_p C_{\mu\nu} \langle p^\mu p^\nu \rangle f^{(0)}(p) \{1 + f^{(0)}(p)\} . \quad (20)$$

Obtaining  $C_{\mu\nu}$  by solving eq. (17) is the most important component of the calculation. Evaluation of the advective derivative of the equilibrium distribution function on the left hand side of this equation results in the integral equation

$$\mathcal{L}[C_{\mu\nu}] = -\langle p_\mu p_\nu \rangle f^{(0)}(p) \{1 + f^{(0)}(p)\} / T \quad (21)$$

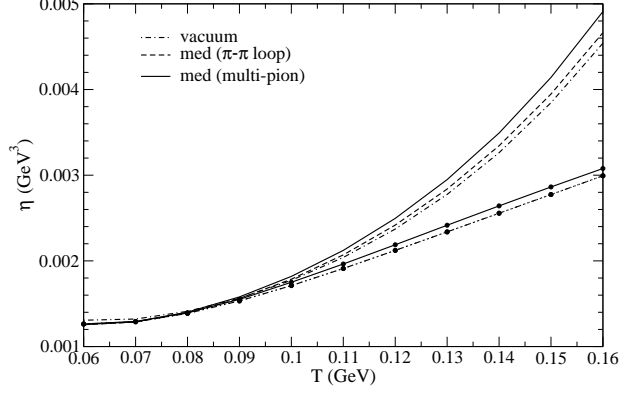


FIG. 4: The shear viscosity as a function of temperature in the Chapman-Enskog approximation. The upper set of curves were obtained with  $\psi_{max} \sim 2$  in eq. 24 where the dash-dotted line indicates use of the vacuum cross-section and the dashed and solid lines correspond to in-medium cross-section for the  $\pi\pi$  and multi-pion cases respectively. The lower set of curves (with circles) were obtained with  $\psi_{max} = \infty$ . Here, the dash-dotted line (with circles) represents the vacuum case and the dashed and solid lines (with circles) correspond to in-medium cross-sections for the  $\pi\pi$  and multi-pion cases respectively. The difference between the corresponding curves in the upper and lower sets is a measure of the uncertainty in  $\eta$  due to insufficient information about the cross-section for energies more than  $\sim 1$  GeV.

which can be reduced to algebraic equations by expanding the unknown function  $C_{\mu\nu}$  in terms of orthogonal polynomials. Similar techniques have been used by many authors to calculate the transport coefficients [6–10, 18]. Using e.g. generalized Laguerre polynomials (of half-integral order) the first approximation to the shear viscosity obtained by keeping the first term in the series is given in the notation of [33, 36] by

$$\eta = \frac{T}{10} \frac{\gamma_0^2}{c_{00}} \quad (22)$$

where

$$\begin{aligned} \gamma_0 &= -10 \frac{S_3^{-2}(z)}{S_2^{-1}(z)} \quad \text{with } z = m_\pi/T \quad \text{and} \\ c_{00} &= I_1(z) + I_2(z) + I_3(z) . \end{aligned} \quad (23)$$

The integrals  $I_\alpha(z)$  are given by

$$I_\alpha(z) = \frac{N_\alpha(z)}{[S_2^{-1}(z)]^2} \int_0^\infty d\psi \cosh^3 \psi \sinh^7 \psi \int_0^\pi d\Theta \sin \Theta \frac{1}{2} \frac{d\sigma}{d\Omega}(\psi, \Theta) \int_0^\infty d\chi L_\alpha(\chi)$$

$$\int_0^{2\pi} d\phi \int_0^\pi d\theta \sin \theta \frac{e^{2z \cosh \psi \cosh \chi}}{(e^E - 1)(e^F - 1)(e^G - 1)(e^H - 1)} M_\alpha(\theta, \Theta) \quad (24)$$

where

$$\begin{aligned} E &= z(\cosh \psi \cosh \chi - \sinh \psi \sinh \chi \cos \theta) \\ F &= z(\cosh \psi \cosh \chi - \sinh \psi \sinh \chi \cos \theta') \\ G &= E + 2z \sinh \psi \sinh \chi \cos \theta \\ H &= F + 2z \sinh \psi \sinh \chi \cos \theta' , \end{aligned} \quad (25)$$

and the functions  $N$ ,  $L$ ,  $M$  and  $S$  are defined as

$$\begin{aligned} N_1(z) &= 16z^4, \quad N_2(z) = 16z^4, \quad N_3(z) = 16z^4/3, \\ L_1(\chi) &= \sinh^2 \chi, \quad L_2(\chi) = \sinh^4 \chi, \quad L_3(\chi) = \sinh^6 \chi, \\ M_1(\theta, \Theta) &= 1 - \cos^2 \Theta, \quad M_2(\theta, \Theta) = \cos^2 \theta + \cos^2 \theta' - 2 \cos \theta \cos \theta' \cos \Theta, \\ M_3(\theta, \Theta) &= [\cos^2 \theta - \cos^2 \theta']^2 \quad \text{and} \\ S_n^\alpha(z) &= \sum_{k=1}^{\infty} k^\alpha K_n(kz). \end{aligned} \quad (26)$$

Here  $K_n(x)$  denotes modified Bessel function of order  $n$  and  $\cos \theta' = \cos \theta \cos \Theta - \sin \theta \sin \Theta \cos \phi$ .

We plot  $\eta$  versus  $T$  in Fig. 4 obtained in the Chapman-Enskog approximation showing the effect of the in-medium  $\rho$  propagation in the pion gas. In the upper set of curves the upper limit of integration over  $\psi$  in eq. (24) is taken to be  $\sim 2$  which corresponds to a center of mass energy ( $E_{c.m.} = 2m_\pi \cosh \psi$ ) of  $\sim 1$  GeV for  $\pi\pi$  scattering up to which we have obtained a fair description of the cross-section using  $\rho$  and  $\sigma$  exchange. Here we observe  $\sim 10\%$  change at  $T = 150$  MeV due to medium effects compared to the vacuum when all the loops in the  $\rho$  self-energy are considered. The effect reduces with temperature to less than 5% at 100 MeV and the curves almost merge with each other as  $T$  reaches  $\sim 60$  MeV. The lower set of curves (with circles) in Fig. 4 depict the corresponding set of curves when the actual upper limit of  $\psi$  (which is  $\infty$ ) is used. The difference between the two set of curves indicates the uncertainty in the results on account of insufficient information of the cross-section at higher energies.

We also present results for the relaxation time approximation which is the simplest way to linearize the transport equation. Here one assumes that  $f(x, p)$  goes over to the equilibrium

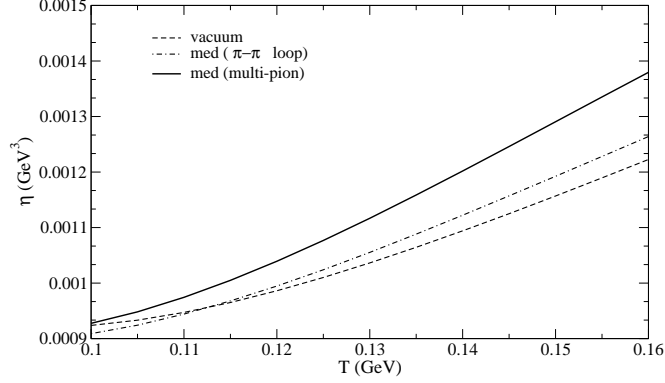


FIG. 5: The shear viscosity as a function of temperature in the relaxation time approximation. The dash-dotted and solid lines correspond to the use of in-medium cross-sections in eq. 27 for  $\pi\pi$  and multi-pion loops respectively. The dashed line represents the vacuum case.

distribution  $f^{(0)}(x, p)$  as a result of collisions and this takes place over a relaxation time  $\tau(p)$  which is the inverse of the collision frequency  $\omega(p)$ . The right hand side of eq. (14) is then given by  $-E_p \omega(p) [f(x, p) - f^{(0)}(x, p)]$ . For collisions of the form  $\pi(p) + \pi(k) \rightarrow \pi(p') + \pi(k')$  we have

$$\omega(p) = \int d\Gamma_k \frac{\sqrt{s(s - 4m_\pi^2)}}{2E_p} f(E_k) (1 + f(E_{p'})) (1 + f(E_{k'})) \frac{1}{2} \int d\Omega \frac{d\sigma}{d\Omega} \quad (27)$$

and the shear viscosity is given by [5, 34, 37, 38]

$$\eta = \frac{1}{15T} \int d\Gamma_p \frac{p^4}{E_p} \tau(p) f(E_p) (1 + f(E_p)) . \quad (28)$$

We show the temperature dependence of  $\eta$  in the relaxation time approximation in Fig. 5. The values in this case are lower than that obtained in the Enskog method though the effect of the medium is larger. The difference depends largely on the energy dependence of the cross-section as noted in [39].

#### IV. SUMMARY AND OUTLOOK

To summarize, we have used an effective Lagrangian approach to evaluate the  $\pi\pi$  scattering cross-section in which the temperature dependence enters through the in-medium propagator of the  $\rho$  which mediates the interaction between the pions. This has been used to evaluate the shear viscosity of a pion gas to the first Chapman-Enskog order. The tem-

perature dependence with and without medium effects shows a noticeable difference in this approach as well as in the relaxation time and non-relativistic approaches.

We end by stating that the main focus in this work has been to emphasize the role of medium modifications of the cross-section in the evaluation of the transport coefficients. The values of  $\eta$  arrived at in the present calculation may be modified in a more realistic scenario employing model independent approaches in the lines of [40]. In addition, the treatment has to be extended to include other mesons and nucleons. Only then can the temperature dependent shear viscosity be included in the hydrodynamics instead of constant values used e.g. in the evaluation of electromagnetic spectra from heavy ion collisions [41]. Such an effort is underway and will be reported in due course.

## V. APPENDIX

Using standard techniques of thermal field theory, the polarization function of the  $\rho$  corresponding to the  $\pi - h(= \pi, \omega, h_1, a_1)$  loop diagrams shown in Fig. 2 is given [22, 23] by

$$\begin{aligned} \Pi^{\mu\nu}(q_0, \vec{q}) = & \int \frac{d^3k}{(2\pi)^3} \frac{1}{4\omega_\pi\omega_h} \left[ \frac{(1+f(\omega_\pi))N_1^{\mu\nu} + f(\omega_h)N_3^{\mu\nu}}{q_0 - \omega_\pi - \omega_h + i\eta\epsilon(q_0)} + \frac{-f(\omega_\pi)N_1^{\mu\nu} + f(\omega_h)N_4^{\mu\nu}}{q_0 - \omega_\pi + \omega_h + i\eta\epsilon(q_0)} \right. \\ & \left. + \frac{f(\omega_\pi)N_2^{\mu\nu} - f(\omega_h)N_3^{\mu\nu}}{q_0 + \omega_\pi - \omega_h + i\eta\epsilon(q_0)} + \frac{-f(\omega_\pi)N_2^{\mu\nu} - (1+f(\omega_h))N_4^{\mu\nu}}{q_0 + \omega_\pi + \omega_h + i\eta\epsilon(q_0)} \right] \end{aligned} \quad (\text{A.1})$$

where  $\omega_\pi = \sqrt{\vec{k}^2 + m_\pi^2}$  and  $\omega_h = \sqrt{(\vec{q} - \vec{k})^2 + m_h^2}$  are the Bose distribution functions. The factor  $N^{\mu\nu}$  contains tensor structures from the vertices and the vector propagators and are given by

$$\begin{aligned} N_{\mu\nu}^{(\pi)}(q, k) &= \left( \frac{2G_\rho}{m_\rho F_\pi^2} \right)^2 C_{\mu\nu} \\ N_{\mu\nu}^{(\omega)}(q, k) &= -4 \left( \frac{g_1}{F_\pi} \right)^2 (B_{\mu\nu} + q^2 k^2 A_{\mu\nu}) \\ N_{\mu\nu}^{(h_1)}(q, k) &= - \left( \frac{g_2}{F_\pi} \right)^2 \left( B_{\mu\nu} - \frac{1}{m_{h_1}^2} C_{\mu\nu} \right) \\ N_{\mu\nu}^{(a_1)}(q, k) &= -2 \left( \frac{g_3}{F_\pi} \right)^2 \left( B_{\mu\nu} - \frac{1}{m_{a_1}^2} C_{\mu\nu} \right) \end{aligned} \quad (\text{A.2})$$

where

$$\begin{aligned} A_{\alpha\beta}(q) &= -g_{\alpha\beta} + q_\alpha q_\beta / q^2, \\ B_{\alpha\beta}(q, k) &= q^2 k_\alpha k_\beta - q \cdot k (q_\alpha k_\beta + k_\alpha q_\beta) + (q \cdot k)^2 g_{\alpha\beta}, \\ C_{\alpha\beta}(q, k) &= q^4 k_\alpha k_\beta - q^2 (q \cdot k) (q_\alpha k_\beta + k_\alpha q_\beta) + (q \cdot k)^2 q_\alpha q_\beta. \end{aligned} \quad (\text{A.3})$$

The interaction Lagrangians used to obtain these are given in [22]. The subscript  $i(= 1, ..4)$  on  $N^{\mu\nu}$  in (A.1) correspond to its values for  $k_0 = \omega_\pi, -\omega_\pi, q_0 - \omega_h, q_0 + \omega_h$  respectively. The imaginary part is easily read off from (A.1) and is given by

$$\begin{aligned} \text{Im}\Pi^{\mu\nu}(q_0, \vec{q}) = & -\pi \int \frac{d^3k}{(2\pi)^3 4\omega_\pi\omega_h} \times \\ & [N_1^{\mu\nu} \{(1 - f(\omega_\pi) - f(\omega_h))\delta(q_0 - \omega_\pi - \omega_h) + (f(\omega_\pi) - f(\omega_h))\delta(q_0 - \omega_\pi + \omega_h)\} \\ & + N_2^{\mu\nu} \{(f(\omega_h) - f(\omega_\pi))\delta(q_0 + \omega_\pi - \omega_h) - (1 - f(\omega_\pi) - f(\omega_h))\delta(q_0 + \omega_\pi + \omega_h)\}] \end{aligned} \quad (\text{A.4})$$

where the factors  $N_{3,4}^{\mu\nu}$  have converted to  $N_1^{\mu\nu}$  or  $N_2^{\mu\nu}$  on use of the associated  $\delta$ -functions. The latter actually define the kinematic domains where different scattering and decay processes leading to the loss or gain of the  $\rho$  mesons in the medium. The non-vanishing regions produce branch cuts in the self-energy function. The first and the fourth terms are non-zero for  $q^2 > (m_h + m_\pi)^2$  giving rise to the unitary cut and the second and third terms are non-vanishing for  $q^2 < (m_h - m_\pi)^2$  giving rise to the Landau cut. Whereas the unitary cut is present in vacuum as well, the Landau cut appears only in the medium.

Performing the angular integration, the unitary and Landau cut contributions for the physically relevant region  $q_0, q^2 > 0$  are obtained respectively as

$$\begin{aligned} \text{Im}\Pi_U^{\mu\nu}(q_0, \vec{q}) = & -\frac{R^2}{32\pi q^2} \int_{-v}^v dx N^{\mu\nu}(x) \{1 + f(\omega) + f(q_0 - \omega)\} \\ & \text{for } q_0 \geq \sqrt{(m_h + m_\pi)^2 + |\vec{q}|^2} \\ \text{Im}\Pi_L^{\mu\nu}(q_0, \vec{q}) = & \frac{R^2}{32\pi q^2} \int_{-v}^v dx N^{\mu\nu}(x) \{f(\tilde{\omega}) - f(q_0 + \tilde{\omega})\} \\ & \text{for } |\vec{q}| \leq q_0 \leq \sqrt{(m_h - m_\pi)^2 + |\vec{q}|^2} \end{aligned} \quad (\text{A.5})$$

where  $x$  is defined in the two cases through  $\omega = (R^2/2q^2)(q_0 + |\vec{q}|x)$  and  $\tilde{\omega} = (R^2/2q^2)(-q_0 + |\vec{q}|x)$  with  $R^2 = q^2 - m_h^2 + m_\pi^2$  and  $v = \sqrt{1 - \frac{4q^2 m_\pi^2}{R^4}}$ . The transverse and longitudinal components for different graphs can now be obtained using the relations,

$$A_\mu^\mu = -3, \quad A_{00} = \frac{|\vec{q}|^2}{q^2} \quad (\text{A.6})$$

$$B_\mu^\mu = m_\pi^2 q^2 + \frac{R^4}{2}, \quad B_{00} = -\frac{|\vec{q}|^2 R^4}{4q^2} (1 - x^2) \quad (\text{A.7})$$

$$C_\mu^\mu = q^2(m_\pi^2 q^2 - \frac{R^4}{4}), \quad C_{00} = \frac{|\vec{q}|^2 R^4}{4} x^2. \quad (\text{A.8})$$

The real parts are obtained as principal value integrals which remain after removal of the imaginary part from eq. (A.1). Note that unlike the imaginary part, the real part of the self-energy at a given value of  $q_0$  receives contribution from all the terms.

To take into account the finite  $3\pi$  and  $\rho\pi$  decay widths ( $\Gamma_h$ ) of the unstable mesons in the loop, the self-energy is folded with their spectral function,

$$\Pi(q, m_h) = \frac{1}{N_h} \int_{(m_h-2\Gamma_h)^2}^{(m_h+2\Gamma_h)^2} dM^2 \frac{1}{\pi} \text{Im} \left[ \frac{1}{M^2 - m_h^2 + iM\Gamma_h(M)} \right] \Pi(q, M) \quad (\text{A.9})$$

$$\text{with } N_h = \int_{(m_h-2\Gamma_h)^2}^{(m_h+2\Gamma_h)^2} dM^2 \frac{1}{\pi} \text{Im} \left[ \frac{1}{M^2 - m_h^2 + iM\Gamma_h(M)} \right].$$

- 
- [1] L. P. Csernai, J. I. Kapusta and L. D. McLerran, Phys. Rev. Lett. **97**, 152303 (2006).
  - [2] P. Kovtun, D. T. Son and A. O. Starinets, Phys. Rev. Lett. **94**, 111601 (2005).
  - [3] P. B. Arnold, G. D. Moore and L. G. Yaffe, JHEP **0011** (2000) 001; **0305** (2003) 051
  - [4] P. B. Arnold, C. Dogan and G. D. Moore, Phys. Rev. D **74** (2006) 085021
  - [5] M. Prakash, M. Prakash, R. Venugopalan and G. Welke, Phys. Rept. **227** (1993) 321.
  - [6] A. Dobado and S. N. Santalla, Phys. Rev. D **65**, 096011 (2002).
  - [7] A. Dobado and F. J. Llanes-Estrada, Phys. Rev. D **69**, 116004 (2004).
  - [8] J. W. Chen, Y. H. Li, Y. F. Liu and E. Nakano, Phys. Rev. D **76**, 114011 (2007)
  - [9] E. Nakano, arXiv:hep-ph/0612255.
  - [10] K. Itakura, O. Morimatsu and H. Otomo, Phys. Rev. D **77**, 014014 (2008).
  - [11] D. Fernandez-Fraile and A. Gomez Nicola, Eur. Phys. J. C **62** (2009) 37; Eur. Phys. J. A **31** (2007) 848.
  - [12] S. Weinberg, Physica A **96** (1979) 327.
  - [13] J. Gasser and H. Leutwyler, Annals Phys. **158**, 142 (1984).
  - [14] R. Rapp, Acta Phys. Polon. B **42** (2011) 2823.
  - [15] S. Ghosh, S. Sarkar and J. Alam, Eur. Phys. J. C **71**, 1760 (2011)
  - [16] S. Sarkar and S. Ghosh, arXiv:1204.0893 [nucl-th].
  - [17] P. Mohanty, V. Roy, S. Ghosh, S. Das, B. Mohanty, S. Sarkar, J. Alam and A. Chaudhuri, Phys. Rev. C **85**, 031903(R) (2012).
  - [18] K. Heckmann, M. Buballa and J. Wambach, arXiv:1202.0724 [hep-ph].
  - [19] F. Klingl, N. Kaiser and W. Weise, Z. Phys. A **356** (1996) 193
  - [20] J. Nieves and E. Ruiz Arriola, Phys. Rev. D **80** (2009) 045023
  - [21] G. Bertsch, M. Gong, L. D. McLerran, P. V. Ruuskanen and E. Sarkkinen, Phys. Rev. D **37** (1988) 1202.

- [22] S. Ghosh, S. Sarkar and S. Mallik, Eur. Phys. J. C **70**, 251 (2010).
- [23] S. Ghosh and S. Sarkar, Nucl. Phys. A **870-871**, 94 (2011)
- [24] M. Le Bellac, *Thermal Field Theory* (Cambridge University Press, Cambridge, 1996).
- [25] S. Mallik and S. Sarkar, Eur. Phys. J. C **61**, 489 (2009).
- [26] K. Nakamura *et al.* [Particle Data Group], J. Phys. G **37** (2010) 075021.
- [27] H. W. Barz, H. Schulz, G. Bertsch and P. Danielewicz, Phys. Lett. B **275** (1992) 19.
- [28] D. N. Zubarev, *Non-equilibrium Statistical Thermodynamics* (Consultants Bureau, NN, 1974).
- [29] A. Hosoya, M. a. Sakagami and M. Takao, Annals Phys. **154** (1984) 229.
- [30] S. Jeon and L. G. Yaffe, Phys. Rev. D **53**, 5799 (1996).
- [31] M. E. Carrington, D. f. Hou and R. Kobes, Phys. Rev. D **64** (2001) 025001.
- [32] S. R. De Groot, W. A. Van Leeuwen and C. G. Van Weert, *Relativistic Kinetic Theory, Principles And Applications* (Amsterdam, Netherlands, North-holland, 1980).
- [33] D. Davesne, Phys. Rev. C **53**, 3069 (1996).
- [34] P. Chakraborty and J. I. Kapusta, Phys. Rev. C **83** (2011) 014906.
- [35] S. Weinberg, Astrophys. J. **168** (1971) 175.
- [36] W. A. Van Leeuwen, P. H. Polak and S. R. De Groot, Physica **66**, 455 (1973).
- [37] S. Gavin, Nucl. Phys. A **435** (1985) 826.
- [38] G. Rupak and T. Schafer, Phys. Rev. A **76** (2007) 053607
- [39] A. Wiranata and M. Prakash, arXiv:1203.0281 [nucl-th].
- [40] A. Dobado, A. Gomez Nicola, F. J. Llanes-Estrada and J. R. Pelaez, Phys. Rev. C **66** (2002) 055201
- [41] S. Mitra, P. Mohanty, S. Sarkar and J. e. Alam, arXiv:1107.2500 [nucl-th].